PCCP

Accepted Manuscript

ROYAL SOCIETY OF CHEMISTRY

www.rsc.org/pccp

Observation of a New Channel, the Production of CH_3, in the Abstraction Reaction of OH Radicals with Acetaldehyde

Neil U. M. Howes, James P. A. Lockhart[†], Mark A. Blitz[1]*, Scott A. Carr, Maria Teresa Baeza-Romero[+], Dwayne E. Heard[1], Robin J. Shannon‡, Paul W. Seakins[1]* and T. Varga[#]

School of Chemistry, University of Leeds, Leeds, LS2 9JT, UK.

[1] National Centre for Atmospheric Science, University of Leeds, Leeds, LS2 9JT, UK.

ABSTRACT: Using laser flash photolysis coupled to photo-ionization time-of-flight mass spectrometry (PIMS), methyl radicals (CH_3) have been detected as primary products from the reaction of OH radicals with acetaldehyde (ethanal, CH_3CHO) with a yield of ~15% at 1-2 Torr of helium bath gas. Supporting measurements based on laser induced fluorescence studies of OH recycling in the $OH/CH_3CHO/O_2$ system are consistent with the PIMS study. Master equation calculations suggest that the origin of the methyl radicals is from prompt dissociation of chemically activated acetyl products and hence is consistent with previous studies which have shown that abstraction, rather than addition/elimination, is the sole route for the OH + acetaldehyde reaction. However, the observation of a significant methyl product yield suggests that energy partitioning in the reaction is different from the typical early barrier mechanism where reaction exothermicity is channeled preferentially into the newly formed bond. The master equation calculations predict atmospheric yields of methyl radicals of ~ 14 %. The implications of the observations in atmospheric and combustion chemistry are briefly discussed.

INTRODUCTION

Acetaldehyde (ethanal, CH_3CHO) is an important atmospheric pollutant formed in the oxidation of many hydrocarbons[1] and also a primary pollutant, particularly from ethanol combustion[2-4] and higher alcohols.[5, 6] Acetaldehyde has been measured in a number of environments at concentrations of sub ppb in remote regions,[7] to tens of ppb in polluted cities.[8-11] Acetaldehyde is a potential carcinogen[12] and, via reaction with the OH radical, a significant source of peroxyacetyl nitrate (PAN):

$$OH + CH_3CHO \rightarrow H_2O + CH_3CO \qquad \Delta_rH = -123 \text{ kJ mol}^{-1} \qquad (1a)$$

$$CH_3CO + O_2 + M \rightarrow CH_3C(O)O_2 + M \qquad (2a)$$

$$CH_3C(O)O_2 + NO_2 + M \rightarrow CH_3C(O)O_2NO_2 + M \qquad (3)$$

PAN is an important component of photochemical smog, a known irritant and a vehicle, via reaction 3, for the long range transport of NOx in the atmosphere.

The kinetics of reaction 1 have been extensively studied; a room temperature rate coefficient of $(1.5 \pm 0.2) \times 10^{-11}$ cm^3 molecule^{-1} s^{-1} has been recommended by IUPAC[13] and $(1.5 \pm 0.1) \times 10^{-11}$ cm^3 molecule^{-1} s^{-1} in the recent JPL evaluation.[14] Following the observation of an upward curvature of the OH + acetone reaction with decreasing temperature below ~200 K, Wollenhaupt et al.[15] suggested that OH + carbonyl reactions may not be simple abstraction reactions. Based on some product studies, *ab initio* calculations and the established negative temperature dependence of reaction 1, it was suggested that addition elimination may compete with abstraction for the reactions of OH with carbonyl species.[16, 17] For the reaction of OH with acetone the channels proposed were:

$$OH + CH_3COCH_3 \rightarrow H_2O + CH_2COCH_3 \quad (4a)$$

$$OH + CH_3COCH_3 \rightarrow CH_3C(O)OH + CH_3 \quad (4b)$$

For the reaction of OH with acetaldehyde the corresponding channels from addition/elimination would be:

$$OH + CH_3CHO \rightarrow CH_3 + HCOOH \qquad \Delta_rH=-103 \text{ kJ mol}^{-1}\ [13] \quad (1b)$$

$$OH + CH_3CHO \rightarrow CH_3C(O)OH + H \qquad \Delta_rH=-86 \text{ kJ mol}^{-1}\ [13] \quad (1c)$$

However, following the suggestion of an alternative reaction mechanism, a number of product studies were undertaken which appeared to confirm that abstraction was either the dominant, or only, channel in the reaction of OH with carbonyl species, and that the upward curvature with decreasing temperature was not associated with a new reaction channel. For example, Vandenberk and Peeters measured the yield of water following the reaction of OH with acetaldehyde and acetone, reporting a yield of 0.89 ± 0.06 for reaction 1[18] and 0.95 for reaction 4.[19] Butkovskaya et al.[20] reported abstraction at ~95% for reaction 1, but determined from observations of the CH_2CHO radical that at 298 K, approximately 5% of the reaction can occur via abstraction from the methyl group of acetaldehyde:

$$OH + CH_3CHO \rightarrow H_2O + CH_2CHO \qquad \Delta_rH=-83 \text{ kJ mol}^{-1}\ [13] \quad (1d)$$

Other groups looked for the expected products of addition/elimination and found little evidence to support a substantive alternative to abstraction. Cameron et al.[21] used UV transient absorption spectroscopy to study both the formation of acetyl (channel 1a) and CH_3 (channel 1b). The primary acetyl yield was determined as 0.93 ± 0.18. A significant methyl yield was observed, but on a longer timescale than acetyl production, and realistic alternative radical-radical mechanisms for CH_3 production were proposed. However, the acetyl UV spectrum is broad and overlaps with the CH_3

spectrum; therefore, there is potential for incorrect assignment of absorptions, especially if vibrational excitation is present in the radical species. Cameron et al. were also unable to observe any H atom production (using resonance fluorescence techniques). Upper limits of 3% and 2% were put on channels 1b and 1c.

Wang et al.[22] used IR transient absorption to determine a water yield of ~100% and set an upper limit on CH_3 of 5%, although on the timescale of their reactions, prompt production of CH_3 can occur from the reaction of $O(^1D)$ with acetaldehyde and from some other unknown source. When O_3 was used as the $O(^1D)$ source, a large additional source of CH_3 was observed and attributed to the reaction of acetyl with O_3:

$$CH_3CO + O_3 \rightarrow CH_3 + CO_2 + O_2 \qquad (5)$$

In addition, Wang et al. used an indirect method to probe for atomic hydrogen production (1c) and, in agreement with Cameron et al., observed no production setting an upper limit of 5% on channel 1c.

There now appears to be a strong consensus that abstraction is the sole mechanism for OH + carbonyl reactions, with recent studies by Shannon et al.[23, 24] accounting for the increase in the rate coefficient at low temperatures. For reaction 1, acetyl production dominates, but with a small yield of vinoxy radical following abstraction at the methyl group. Finally, the role of water in mediating the reaction has been explored by Vöhringer-Martinez et al.[25]

However, D'Anna et al.[26] raised the possibility of a further reaction channel (1e) following abstraction; the production of $CH_3 + CO + H_2O$, still consistent with 100% H_2O formation, but where some of the acetyl would fragment:

$$OH + CH_3CHO \rightarrow CH_3 + CO + H_2O \qquad \Delta_rH=-77 \text{ kJ mol}^{-1} \qquad (1e)$$

Using a smog chamber system, with OH being generated from alkyl nitrite photolysis in synthetic air, D'Anna et al. observed 10% production of CO and HCHO, with HCHO being the expected stable product of methyl radical oxidation in the presence of NOx. The activation energy of acetyl decomposition is ~71 kJ mol^{-1} [27] so there is sufficient exothermicity in reaction 1a (-123 kJ mol^{-1}) for acetyl decomposition to occur in a chemically activated process, although this would require deposition of a significant fraction of the reaction exothermicity into the acetyl fragment. Generally abstraction reactions are associated with partitioning exothermicity predominantly into the newly formed bond (H_2O in this case)[28], however, D'Anna et al. also carried out *ab initio* calculations which showed that there is a post-reaction complex which might serve to facilitate a more statistical distribution of the

reaction exothermicity between the final products. More recent calculations by Mendes et al.[29] confirm the presence of a significant post-reaction complex.

Experimental support for partitioning reaction exothermicity into spectator bonds comes from our earlier studies on the reaction of OH with methylglyoxal[27] and glyoxal.[30] Following abstraction of the aldehydic hydrogen atom from methylglyoxal, the resulting $CH_3C(O)CO$ radical is expected to rapidly thermally decompose to acetyl + CO. In the presence of excess oxygen one would then expect to see OH regeneration at low total pressures from the acetyl + O_2 reaction.[31, 32]

$$CH_3CO + O_2 \rightarrow OH + \text{co-products} \quad (2b)$$

OH regeneration was observed, but the Stern Volmer analysis yielded an intercept higher than the expected unity value, suggesting less than 100% acetyl formation. Baeza-Romero et al.[27] showed that the observed results could be explained if the $CH_3C(O)CO$ fragment retained sufficient energy not only for initial fragmentation, but additionally for some of the acetyl to decompose, preventing complete OH recycling. Similar conclusions can be drawn from our work on the reaction of OH with glyoxal where prompt decomposition of a fraction of the HC(O)CO prevents OH recycling from the HC(O)CO + O_2 reaction:[30, 33]

$$OH + HC(O)C(O)H \rightarrow H_2O + HC(O)CO \quad (6)$$

$$HC(O)CO \rightarrow HCO + CO \quad (7)$$

$$HC(O)CO + O_2 \rightarrow OH + CO_2 + CO \quad (8)$$

In this current work we have investigated the title reaction with two experimental methodologies. Laser flash photolysis coupled to photoionization mass spectrometry (PIMS)[34, 35] has been used to positively identify CH_3CO and CH_3 as primary reaction products. At our photoionization energy, CH_3CO fragmentation occurs and CH_3 was detected from acetyl photo-fragmentation, as well as a primary reaction product. Evidence is presented to show that it is possible to differentiate between primary and fragmentation production. To help confirm our findings, we have also used the acetyl + O_2 reaction[32] in a similar fashion to our earlier work on methylglyoxal, to show that there is less than 100% acetyl production. This method does not identify the products and only determines the total non-acetyl yield. Finally, we have used the master equation package MESMER[36] (Master Equation Solver for Multi-Energy Well Reactions) to explore chemically activated acetyl fragmentation.

EXPERIMENTAL

Laser flash photolysis/photoionization mass Spectrometry Studies

Details of the laser flash photolysis/photoionization mass spectrometry system can be found in the electronic supplementary information (ESI) and previous publications.[34, 35] Briefly, the system comprised of a 70 cm long, 1.25 cm diameter, stainless steel flowtube which was illuminated by a pulsed excimer laser. The OH or Cl radical precursors, substrate and helium bath gas were metered through calibrated flow controllers and mixed prior to entering the flowtube. The total pressure in the flowtube was controlled by a rotary pump and measured using a 10 Torr Baratron-type pressure gauge. Experiments were run with both coated (halocarbon wax) and uncoated flow tubes.

The central region of the flowtube passed through an evacuated chamber ($<10^{-5}$ Torr typical background pressure). A 1 mm hole in the wall of the flowtube allowed the reaction mixture to enter the chamber where it was exposed to pulsed VUV radiation at 118 nm, generated from frequency tripling 355 nm YAG output, which allowed photoionization of compounds with a threshold ionization energy of less than 10.5 eV. Ions generated by the VUV laser pulse were focused into a reflectron time of flight mass spectrometer (ToFMS, Kore Instruments) and were detected via dynode detectors. Ion signals were monitored on a digital oscilloscope and then passed to a PC for analysis.

The time delay between the excimer photolysis laser and the photoionization probe laser was varied to build up a temporal profile of monitored species with typically two hundred points per trace. The experiment was allowed to average over 10-15 scans, to increase the signal to noise ratio.

Studies were carried out under pseudo-first-order conditions with acetaldehyde in a large excess over the radical. Under these conditions the acetyl and methyl radicals generated in the flowtube demonstrated biexponential behavior with a growth determined by the pseudo-first-order rate coefficient for reaction with acetaldehyde, k'_g, and a loss determined by a combination of removal processes, primarily diffusion to the flowtube wall which could be approximated to a first-order loss, k_l. The temporal profile of the ion signal ($S_{X,t}$) is given by equation E1, where the first part of the equation is the bimolecular profile modified by the sampling process and the second part of the equation allows for any prompt production of acetyl or methyl.

$$S_{X,\ t} = \frac{S\, k_g k_{eff}}{k_l - k_g}\left[\frac{e^{-k_g t} - e^{-k_{eff} t}}{k_{eff} - k_g} - \frac{e^{-k_l t} - e^{-k_{eff} t}}{k_{eff} - k_l}\right] + \frac{S_{instant}\, k_{eff}}{k_{eff} - k_l}\left[\frac{e^{-k_l t} - e^{-k_{eff} t}}{k_{eff} - k_l}\right] + S_0 \qquad \text{(E1)}$$

S is proportional to the maximum height of the signal, k_g is the coefficient rate of growth of the signal, k_l is the rate coefficient for the loss rate, k_{eff} is the rate of effusion into the mass spectrometer, $S_{instant}$ refers

to any instantaneous observed (photolytic), S_0 is the signal at time zero, and t is time. Typical CH_3 and CH_3CO signal traces from reaction 1 (where $S_{instant}=0$) are shown in Figure 1.

Branching ratios from kinetic studies with excess oxygen

This component of the work has been carried out in two conventional slow-flow, laser flash photolysis, laser induced fluorescence (LIF) apparatus that have been used in several previous publications.[2, 37, 38] In both systems the flows of hydroxyl radical precursor, acetaldehyde and bath gas (He, He/O_2, N_2, N_2/O_2) were regulated via calibrated mass flow controllers, mixed and flowed into a stainless steel 6-way cross reactor. For ambient and low temperature studies, the reactor had been welded into a metal bath such that just the end flanges of the cell arms protrude through the walls of the bath. Low temperature measurements at 212 K were obtained by filling the bath with chloroform/dry ice. For studies at 385 K, a different reactor was heated with a ceramic oven which was custom made to fit around the central portion of the reaction cell. The total pressure in the cells (1– 60 Torr) was regulated via a needle valve on the output line to the pump and measured using a capacitance manometer. The temperature close to the reaction zone was measured using K-type thermocouples.

OH radicals were generated from the excimer laser pulsed photolysis of t-butyl hydroperoxide at 248 nm.[39]

$$t\text{-}C_4H_9OOH + h\nu \rightarrow OH + \text{co-products} \qquad (P1)$$

Photolysis energies were typically 30 - 100 mJ $pulse^{-1}$, the laser beam had an area of ~ 1 cm^2 and was introduced through one of the arms of the reactor. The laser was typically operated at 10 Hz, although some studies were carried out at lower repetition rates to check that fresh gas was present for each photolysis pulse.

OH radicals were detected by off-resonance LIF (details in the ESI). The time delay between the photolysis and probe lasers was controlled by home-written software and was varied to build up a record of the OH signal following photolysis. Kinetic traces (e.g. inset to Fig 5) were typically 200 – 400 data points each averaged 2 - 10 times depending on the signal-to-noise ratio.

RESULTS

Initial PIMS Results Demonstrating CH_3 Production

Many previous product studies on reaction 1 have operated under conditions where there is no time resolution on the reaction products. In these circumstances it is not possible to temporally correlate reagent removal with product production. However, in our PIMS studies the primary reaction has been isolated and Figure 1 shows an example of the acetyl and methyl signals recorded in the same experiment. Clearly there can be no doubt that they originate from the same source.

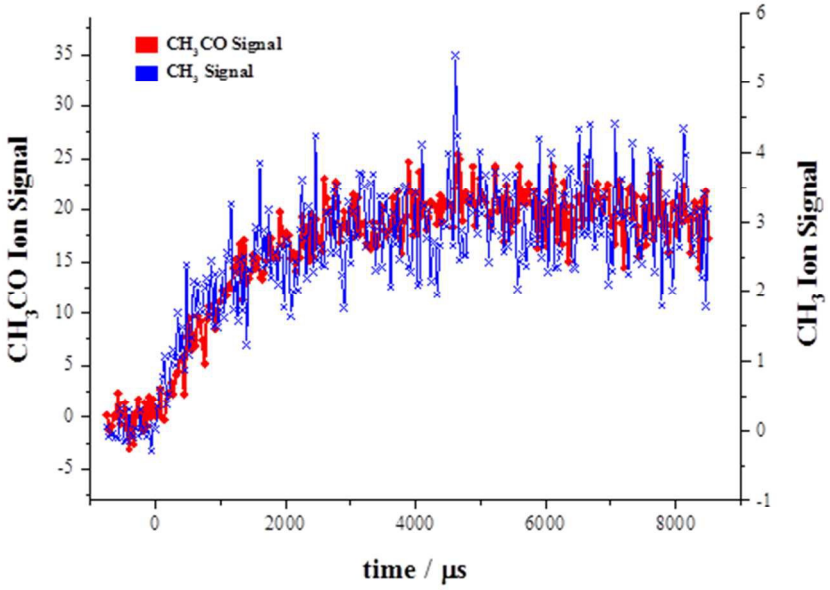

Figure 1. Overlaid plots of acetyl (♦) and methyl (×) signal from the same experiment (1.5 Torr He, N_2O/H_2O as the OH source, $[CH_3CHO] = 4 \times 10^{13}$ molecule cm^{-3}) showing that they are produced on the same timescale.

However, Figure 1 in itself does not confirm methyl as the direct product of reaction 1 as methyl ions are formed during the acetyl photoionization process. Figures 2 and 3 qualitatively show that acetyl fragmentation is not the sole source of methyl ion signal. In Figure 2 the ratio of signal height (the *S* parameter from E1) at *m/z* 15 (CH_3): *m/z* 43 (acetyl) is shown with acetyl radicals being generated from the reactions of OH or Cl with acetaldehyde:

$$Cl + CH_3CHO \rightarrow HCl + CH_3CO \qquad \Delta_rH=-57 \text{ kJ mol}^{-1}\ ^{13} \qquad (9)$$

The higher ratio from reaction 1 is explained by the fact that acetyl radicals produced from reaction 9 do not possess sufficient energy (requires 71 kJ mol^{-1}) to fragment further to CH_3 and CO. The 15:43 ratio from reaction 9 is therefore solely due to fragmentation in the photoionization process. However, in

reaction 1 the 15:43 ratio is higher as the m/z 15 signal is produced both by fragmentation and by methyl radical production from reaction 1.

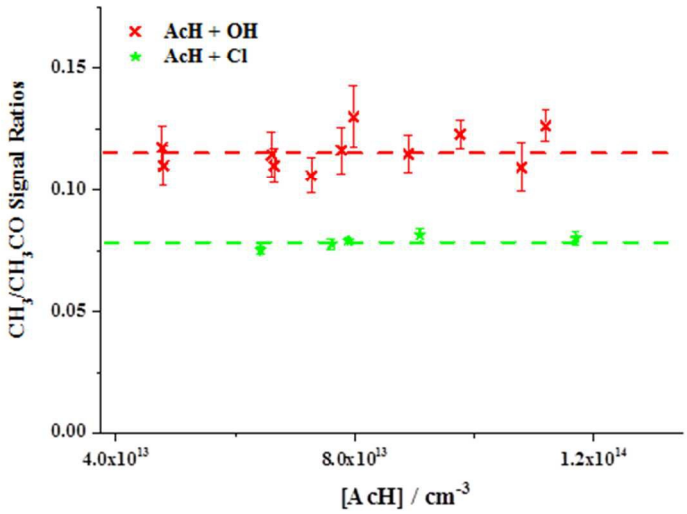

Figure 2. Methyl:acetyl signal ratios following the reaction of OH with acetaldehyde (AcH) and Cl with acetaldehyde. The dashed lines are the average values in these experiments.

In Figure 3, a small amount of oxygen (~10 mTorr) was present in the system and hence a significant fraction of the acetyl that survived fragmentation in reaction 1e formed energized acetylperoxy radicals (reaction 2b) which under the low pressures of the PIMS flowtube (~ 1.5 Torr) yielded OH and a lactone (observable in our system as m/z = 42) with virtually 100% yield.[32] The OH went on to react with acetaldehyde forming a chain system where radicals are maintained for several ms. Each time the chain was propagated a fraction of reaction 1 generated methyl, which accumulated (as $CH_3 + O_2$ was slow under these conditions) whilst the primary acetyl product was recycled. Figure 3 shows the methyl and acetyl radical concentrations which clearly behave very differently as a function of time. The solid lines in Figure 3 are simulations from a numerical model of the system, details of which are given in Section 3.0 of the ESI. Whilst we have fitted the magnitudes of the signals to the observed data (as sensitivity factors are not available for lactones etc), no attempt has been made to fit the temporal behavior of the signals. Given the uncertainties in some of the rate coefficients and in the concentration of O_2, we believe the agreement to be satisfactory. The main result from Figure 3 is that the CH_3 and CH_3CO signals show different temporal profiles demonstrating that fragmentation is not the sole source of the *m/z*=15 signal.

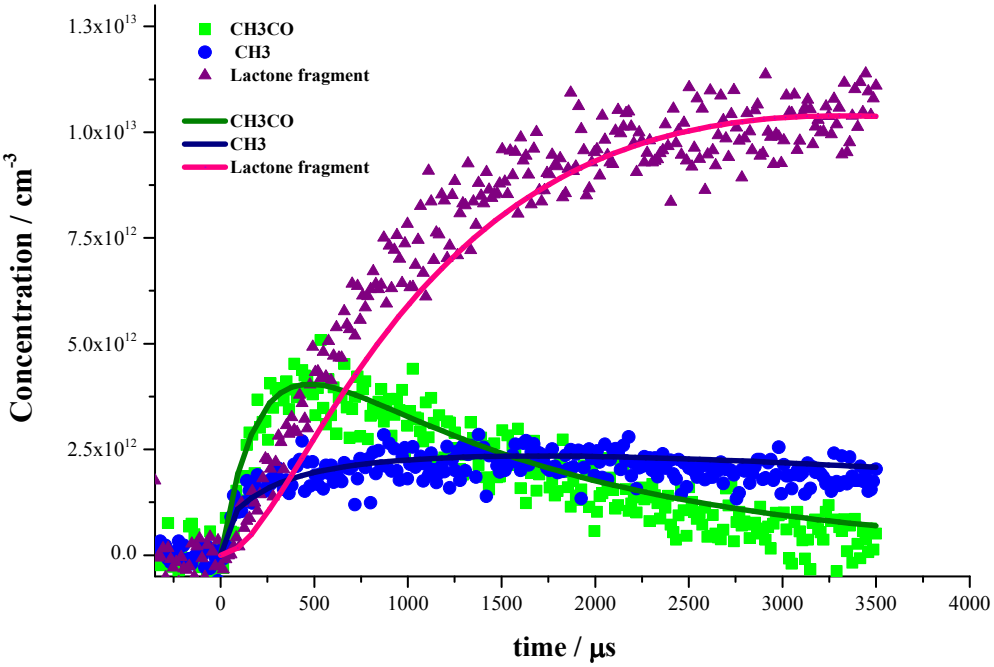

Figure 3. Behavior of acetyl, methyl and lactone signals in an OH/CH_3CHO/O_2 system. The solid points are the experimental data and the lines are a numerical simulation based on a kinetic model. Details of the model can be found in the ESI.

Quantitative Methyl Radical Yields from Reaction 1 using the PIMS system

i) *Kinetics* – The PIMS apparatus can be used to obtain quantitative data on the kinetics of OH and Cl reactions with acetaldehyde. OH radicals were generated indirectly following the reaction of $O(^1D)$ with water:

$$O(^1D) + H_2O \rightarrow 2OH \quad (10)$$

with $O(^1D)$ being generated from either the 248 nm photolysis of ozone or the 193 nm photolysis of N_2O:

$$O_3 + h\nu\ (248\ nm) \rightarrow O_2 + O(^1D) \quad (P2)$$

$$N_2O + h\nu\ (193\ nm) \rightarrow N_2 + O(^1D) \quad (P3)$$

Water is the ideal hydrogen source for OH generation as, in comparison to other potential sources, e.g. H_2, the co-product of reaction 10 is also OH and water is an excellent vibrational quencher of OH.

Figure 4a shows an example of a bimolecular plot for the OH + acetaldehyde reaction where OH has been generated from the 248 nm photolysis of an ozone/water precursor and the reaction was followed by monitoring acetyl radical production. Examples of other data are presented in Table 1 and

compared with literature data. Figure 4b shows an example of a bimolecular plot for Cl + acetaldehyde. Relatively low concentrations of acetaldehyde have been used so that the resulting pseudo-first-order rate coefficients are generally less than 8000 s^{-1} meaning that minimal corrections need to be made to the data to account for transport effects.[34] Agreement with the literature is within the combined experimental uncertainty in all cases. The kinetic data are in good agreement with the literature and encompass a range of different measurement regimes including different precursors, detectors, laser powers, and coated/uncoated reactor walls. The precision of the measurements is somewhat lower than that from experiments in which the removal of OH or Cl is measured, but this is typical of a majority of studies where products are monitored. The good agreement with the literature demonstrates that the target reactions have been isolated and are well characterized.

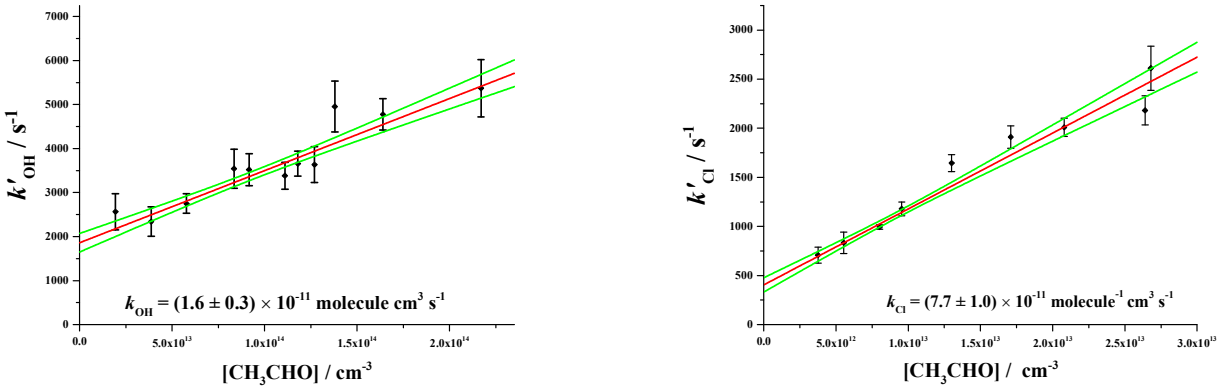

Figure 4. Bimolecular plots of (a) OH + CH_3CHO, (b) Cl + CH_3CHO monitoring acetyl production.

Table 1. Measured Rate Coefficients for Reactions 1 and 9

OH + CH_3CHO		Cl + CH_3CHO	
Set up	10^{11} k_1 [a]	Set up	10^{11} k_9 [a]
O_3[b], OD[c],	2.0 ± 0.2	248 nm[f], OD	6.3 ± 0.7
O_3, OD	1.6 ± 0.3	193 nm, OD	8.6 ± 1.0
O_3, OD	1.5 ± 0.7	193 nm, ND	8.2 ± 2.2
O_3, OD	1.6 ± 0.3	193 nm ND	7.7 ± 1.0
N_2O[d], OD	1.2 ± 0.2		
N_2O, ND[e]	1.4 ± 0.3		
Average	1.6 ± 0.2	Average	7.7 ± 0.7
Literature[13]	1.5 ± 0.2	Literature	8.0 ± 1.4

[a] units cm^3 $molecule^{-1}$ s^{-1}. [b] $O(^1D)$ from O_3 photolysis at 248 nm. [c] Old Detector. [d] $O(^1D)$ from N_2O photolysis at 193 nm. [e] New Detector. [f] Cl generated from oxalyl chloride photolysis at either 248 or 193 nm.

ii) *Methyl Fragmentation Ratios @ 248 nm* – Figure 2 clearly shows a raised CH_3:CH_3CO ratio when OH reacts with acetaldehyde in comparison to Cl reactions, however the ratio of signals cannot be simply used to calculate the direct production of methyl radicals from reaction 1e as the ionization efficiencies of CH_3^+ from fragmentation of acetyl and from methyl itself will not be the same. Calibration was performed by using acetyl chloride as the Cl photolysis source (248 nm) in the presence of acetaldehyde and comparing the prompt acetyl and methyl signals with those produced at longer times from the Cl + acetaldehyde reaction. In the photolysis step the CH_3 signal comes from both direct methyl production and CH_3CO fragmentation. At longer times the CH_3 is solely from the fragmentation of CH_3CO formed from reaction 9. Details of the calibration procedure can be found in the ESI.

$$CH_3C(O)Cl + h\nu \rightarrow CH_3CO + Cl \qquad (\varphi 4a = 0.45) \qquad \text{(P4a)}$$

$$\rightarrow CH_3 + CO + Cl \qquad (\varphi 4b = 0.55) \qquad \text{(P4b)}$$

Using this method a methyl radical yield of (15.5 ± 6.1) % was determined for reaction 1.

iii) *Methyl Fragmentation Ratios @ 193 nm* – For the experiments performed using 193 nm photolysis a different methodology was used to calculate the yield of CH_3 from acetyl decomposition. Here, the

photolytic behavior of acetone at 193 nm, which is well understood[40], was used to determine the yield of methyl radicals.

$$CH_3C(O)CH_3 + h\nu\ (193\ nm) \rightarrow 2CH_3 + CO\ (\varphi \geq 0.95) \qquad (P5)$$

As with the experiments performed at 248 nm, the ethanal + OH and ethanal + Cl reactions were investigated. However, at 193 nm these experiments were carried out back-to-back with some acetone photolysis experiments. Further information is available in the ESI.

For these experiments a yield of methyl radicals of (14.2 ± 2.4) % was determined. The calculated yield is not significantly different from the methyl radical yield determined at 248 nm, so the two methodologies used appear to compare well to each other. A full list of all the experiments performed is presented using in Table 2.

In the photolysis experiments a potential complication could arise if not all the $O(^1D)$ reacted with water or if any vibrationally excited OH were to react with acetaldehyde. Details of experiments to investigate the magnitude of any such corrections can be found in the ESI and the slightly amended values for the CH_3 yields are presented in the last column of Table 2 (Note: correction factor may be a overestimation of the $O(^1D)$ contribution).

Table 2. Methyl Radical Yields from the OH + CH_3CHO reaction.

Method	**CH_3 Yield (%)**	**Corrected CH_3 Yield (%)**
Preliminary data (N_2O)*	19.9 ± 60	17.3 ± 3.0
O_3, OD	15.5± 6.1	14.2 ± 5.8
N_2O, OD	17.1 ± 2.9	14.5 ± 2.0
N_2O, ND	14.2 ± 2.4	11.9 ± 1.8
Average (±2σ)	**15.6 ± 2.9**	**13.5 ± 2.8**

*data excluded from average.

OH yields from kinetic analysis of the OH+CH_3CHO reaction with and without additional oxygen

The kinetic studies of reaction 1 (with or without additional oxygen) were carried out under pseudo-first-order conditions such that the concentration of acetaldehyde (and oxygen if used) was always in

great excess over the OH. Under these conditions, with nitrogen (or helium) as the bath gas, OH removal is determined by the following reactions:

$$OH + CH_3CHO \rightarrow H_2O + \text{co-products} \quad (1)$$

$$OH \rightarrow \text{loss} \quad (11)$$

where reaction 11 accounts for the reaction of OH with the precursor or diffusion out of the observation region. The time dependence of the OH signal I_f is given by:

$$I_f(t) = I_f(0)e^{-k't} \quad (E2)$$

where $I_f(0)$ is the initial OH signal and $k' = k_1[\text{acetaldehyde}] + k_{11}$ and therefore k_1 is the gradient of a bimolecular plot (k' vs [acetaldehyde]), an example of which can be seen as the upper line in Figure 5.

In the presence of molecular oxygen, acetyl formed in reaction 1a will react with O_2, with a fraction regenerating OH (e.g. reaction 2b) as described above. A schematic of the acetyl + O_2 system is shown below:

$$CH_3CO + O_2 \rightarrow CH_3C(O)O_2^* \rightarrow OH + \text{co-products}$$

$$[M] \downarrow k_M$$

$$CH_3C(O)O_2$$

If the concentration of O_2 is such that the acetyl + O_2 reaction is fast compared to the OH + acetaldehyde reaction ($k'_2 > 10k_1$), then under these conditions, the OH chemical removal will be determined by fraction of reaction 1 that does not regenerate OH. The bimolecular rate coefficient for OH loss in the presence of oxygen, k_{O2}, will be reduced compared to nitrogen, k_{N2}, (see lower traces in Figure 5). The yield of OH, ΦOH, is given by:

$$\Phi_{OH} = 1 - \frac{k_{O_2}}{k_{N_2}} \quad (E3)$$

OH yields from reaction 1 were determined as a function of pressure at 212, 298 and 385 K. Φ_{OH} decreases with increasing pressure due increased collisional deactivation of the initially excited $CH_3C(O)O_2^*$ adduct and Φ_{OH} can be parameterized with a Stern Volmer analysis (Φ_{OH}^{-1} vs [M]) where the gradient is ratio of rate coefficients for $CH_3C(O)O_2^*$ forming OH and being stabilized (k_M/k_r) and the intercept is Φ_{OH}^{-1} at zero pressure. For the $CH_3CO + O_2$ system all studies[e.g. 41, 42] have shown unit intercept, i.e. $\Phi_{OH} = 1$ at zero pressure.

Figure 6 shows the Stern Volmer plots for the three temperatures studied and the results are tabulated in Table 3. In all cases the confidence intervals for the intercept do not include, and are greater

than unity (1.04 – 1.36). An intercept > 1 suggests that a fraction of the reaction 1 is generating a product which does not regenerate OH in the presence of O_2 at low total pressures. For 298 K, the fraction of reaction (1) not regenerating OH is (18 ± 5) %.

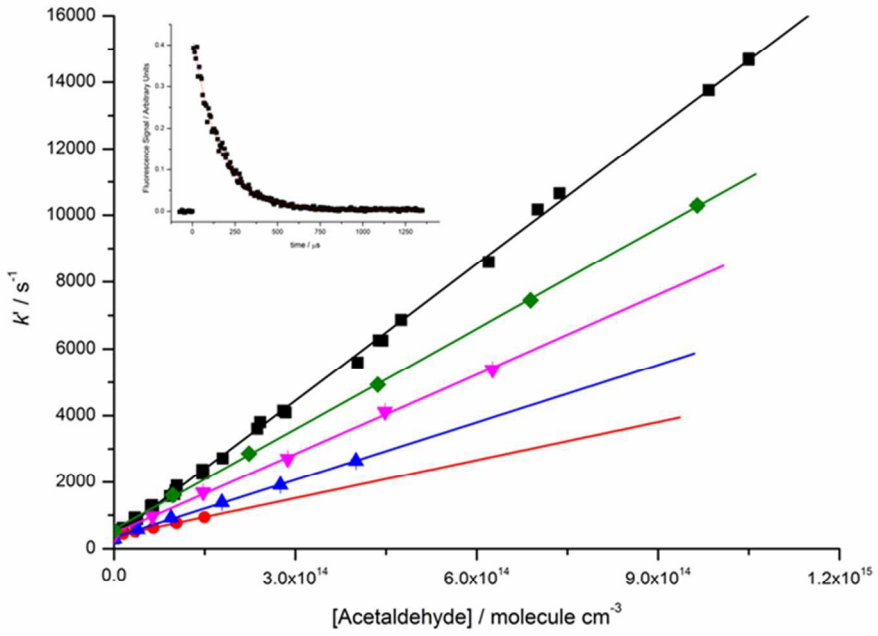

Figure 5. Bimolecular plots at 298 K. (■) = no oxygen, (♦) 10 Torr O_2 , (▼) 5 Torr O_2 , (▲) 2 Torr O_2, (●) 1 Torr O_2; error bars are purely statistical at the 2σ level.

Table 3. Rate coefficients and Stern Volmer parameters determined for reaction 1.

Temperature /K	10^{11} k_1[a]	Intercept	Max and Min Intercept	10^{18} gradient[c]
212	2.07±0.31[b]	1.20	1.33	9.1±1.3[b]
			1.06	
298	1.35±0.13	1.18	1.23	7.57±0.32
			1.13	
385	1.27±0.24	1.20	1.36	4.53±0.26
			1.04	

[a] units cm^3 $molecule^{-1}$ s^{-1}. [b] 2σ statistical error. [c] units cm^3 $molecule^{-1}$

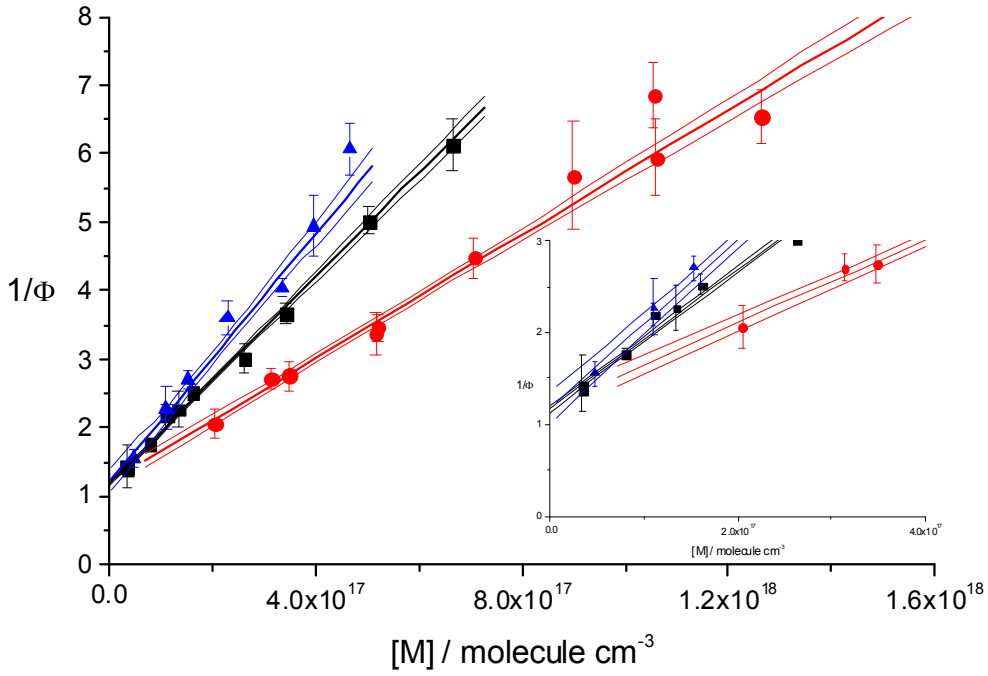

Figure 6. Stern Volmer plots of the reciprocal of the OH yield vs total pressure of nitrogen. (▲) = 212 K, (■) = 298 K, (●) = 385 K. Outlying lines are 95% confidence limits.

As shown in Table 3, the bimolecular rate coefficients measured for reaction 1 are in good agreement with the recommended literature values[13] and the measured gradient of the Stern-Volmer plot at 298 K is in reasonable agreement with earlier work from Tyndall et al.[43] As would be expected the gradient of the Stern-Volmer plot, the ratio of the rate coefficient for OH formation from chemically activated $CH_3C(O)O_2$ to that of stabilization, decreases with increasing temperature.

Master Equation Calculations

In order to support the experimental observations, master equation calculations were performed using the open source code MESMER (http://sourceforge.net/projects/mesmer/). This software, and the basic techniques it uses to solve the chemical master equation, have been well documented elsewhere[36] and will not be discussed further in the current work.

One aspect of the MESMER functionality which is used in the current work, and does warrant additional discussion, is the use of a prior distribution statistical model in order to calculate the activated energy distribution in the CH_3CO radical following hydrogen abstraction from CH_3CHO by OH. A prior

distribution is one extreme example of how reaction exothermicity can be distributed and is usually applied to reactions proceeding via the formation of a long-lived complex. As described below, the prior distribution of energy had to be modified to selectively channel energy into the H_2O fragment (i.e. closer to the dynamical picture where energy is partitioned into the newly formed bond).

The probability the CH_3CO product is formed with energy E (P(E)) is given by the following expression[44]:

$$P(E) = \frac{\rho(E)[\rho_t \otimes \rho_{H_2O}](E_x - E)}{[\rho_{CH_3CO} \otimes \rho_t \otimes \rho_{H_2O}]E_x} \quad \text{(E4)}$$

where E_x is the exothermicity of the CH_3CHO + OH reaction, ρ_{H3CO} is the ro-vibrational density of states of CH_3CO, ρ_t is the classical translational density of states of the CH_3CO and H_2O fragments, ρ_{H2O} is the ro-vibrational density of states of the H_2O co-product and $\otimes$ represents a convolution. In this work the classical translational density of states is used with $\rho_t \propto E$.

In order to refine both the exothermicity of the CH_3CHO + OH reaction and the activation energy for the C-C bond dissociation in CH_3CO, electronic structure theory calculations were performed. These consisted of geometry optimizations at the M062x/6-311+(3df,2pd) level of theory[45] using the Gaussian 09 suite of software[46] followed by single point energy calculations at the ROHF-UCCSD(T)-f12b/aug-cc-pVQZ level of theory using Molpro.[47] From these calculations E_x was determined to be 124.9 kJ mol^{-1} and the saddle point energy for the dissociation of CH_3CO was determined to be 61.7 kJ mol^{-1} including a zero point energy correction. In addition, in both CH_3CO and the corresponding dissociation transition state (TS1), one of the vibrational normal modes corresponds to an internal hindered rotation, and hindrance potentials for each of these were calculated using relaxed scans at the M062x/6-31+G** level of theory. Values for $\langle \Delta E_{down} \rangle$ of 150 cm^{-1} and 300 cm^{-1} were used for He and N_2 respectively.[48]

To account for the loss of the CH_3CO radical due to reaction with O_2 in MESMER, the reaction was treated as a pseudo-isomerization using the methodology recently developed by Green and Robertson.[49] This approach allows bimolecular reactions to be included in the master equation in a fully reversible manner such that detailed balance is satisfied. Additional master equation calculations were performed in order to explore the way in which the internal energy of the CH_3CO radical affected the product yields upon addition of O_2. For these calculations, the potential energy surface from a previous publication on the CH_3CO + O_2 reaction was used.[32] The master equation calculations were performed exactly as described previously with the exception that the CH_3CO fragment was initialized with a prior distribution of energy as described above.

DISCUSSION

Our results from the PIMS measurements of methyl yields and the more indirect kinetic studies generate consistent results. In combination with master equation calculations, zero pressure yields of 12 – 20% have been measured for the fraction of reaction 1 leading to CH_3 + CO + H_2O. These results are in agreement with a majority of previous product studies which conclude that abstraction is the dominant mechanism, but conflict with a model of a classical abstraction process and with the methyl yield determinations of Wang et al.[22] and Cameron et al.[21] These are not easy experiments and therefore we have tried to ensure that our PIMS results are not subject to systematic errors by using different OH precursors and repeating the experiments under a range of different conditions (e.g. coated or uncoated walls, different detectors, wide range of acetaldehyde concentrations, varying radical densities), and by ensuring that we can reproduce literature values for OH and Cl rate coefficients with acetaldehyde.

The qualitative data on the PIMS methyl yields clearly show that methyl radicals are not solely generated from acetyl fragmentation and therefore the correlation in the kinetics between methyl and acetyl production demonstrates that methyl is being generated directly from reaction 1. There are other possible sources of methyl radicals (detailed in the ESI); for example if insufficient water is added, then acetaldehyde can compete with water for the $O(^1D)$ produced from ozone or nitrous oxide photolysis:

$$O(^1D) + CH_3CHO \rightarrow CH_3 + \text{co-products} \quad (12)$$

However, the fast timescale of $O(^1D)$ chemistry means that methyl radicals produced in this way will appear as an instant growth rather than on the same time scale as acetyl radicals. Conversely, because of the low overall radical concentrations, any radical-radical reactions leading to methyl production would occur on much longer timescales than acetyl generation. However, the yield of methyl radical determined would be dependent on acetaldehyde concentration and this was not observed experimentally. Additionally, the potential for interference from vibrationally 'hot' OH was also investigated (see supplementary information for details), with the modeling of this effect suggesting an [acetaldehyde] dependency which was not observed experimentally. The results from the modeling of these reaction channels implies that the dominant source of methyl radicals is the chemically activated decomposition of acetyl radicals.

The kinetic studies are more indirect in nature, but are complementary to the more direct observation of methyl yields and thus help to eliminate possible systematic errors. For example reaction 5, ($CH_3CO + O_3$) could be a source of methyl in some of the PIMS experiments, but no ozone is present

in the kinetic studies. The increase in the intercept of the Stern Volmer plot above unity merely gives a measure of the fraction of the reaction 1 that does not recycle OH radicals, predominantly via reaction 2, ($CH_3CO+O_2 \rightarrow OH+$co-products). Channel 1e ($CH_3 + CO + H_2O$) is one possibility, but another is the abstraction from the methyl group of acetaldehyde, reaction 1d, generating the vinoxy radical:

$$OH + CH_3CHO \rightarrow H_2O + CH_2CHO \quad (1d)$$

with a yield of ~5% determined by Butkovskaya et al.[20], a value which cannot account for our observations (which suggests an (13.5 ± 2.8) % non-OH recycling component from the PIMS studies) and additionally the reaction of vinoxy with O_2 may actually regenerate OH via reaction 13.[50, 51]

$$CH_2CHO + O_2 \rightarrow OH + HCHO + CO \quad (13)$$

Reactions 13 and 14-16 would also provide a partial explanation for the results of D'Anna et al.[26] who observed a 10% yield of HCHO and CO in a chamber study at 760 Torr.

$$CH_2CHO + O_2 \rightarrow OOCH_2CHO \quad (14)$$

$$OOCH_2CHO + NO \rightarrow OCH_2CHO + NO_2 \quad (15)$$

$$OCH_2CHO (+O_2) \rightarrow HCHO + HO_2 + CO \quad (16)$$

However, once again, the observed yield of HCHO and CO is greater than the initial vinoxy yield from reaction (1d).

Not surprisingly, when performing master equation calculations on the dissociation of the activated CH_3CO radical, it was found that partitioning the exothermicity from the CH_3CHO + OH reaction (-123 kJ mol^{-1}) on a purely statistical basis over predicted the yield of CH_3 and CO, giving a branching ratio of 83%. In order to model the experimental data, it was found that the amount of energy deposited in the CH_3CO needed to be reduced. The prior distribution was altered though increasing the density of states of the H_2O and vibrational modes were added to this species until MESMER simulations in 1.5 Torr of He predicted a dissociation yield of ~14 %, in agreement with experiment. Vibrational energy distributions from the modified prior distribution are shown in Figure 7. Note the good agreement between the peak of the calculated water distribution and the average internal energy of water measured by Butkovskaya and Setser.[52]

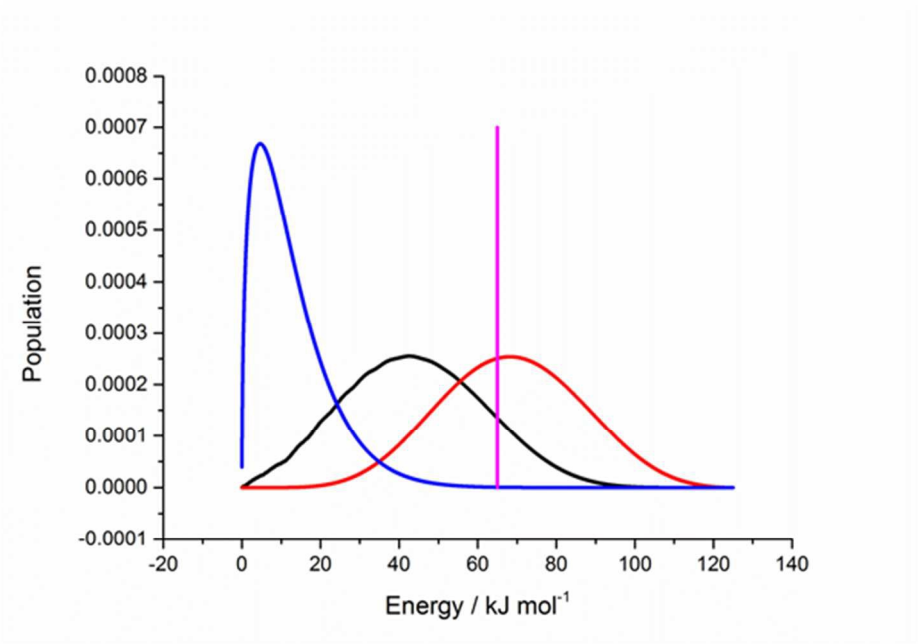

Figure 7. Energy distributions in acetyl (black line), H_2O (red line) and in translational motion of the fragments (blue line) calculated using a prior distribution calculation modified to give 13.6% acetyl fragmentation at 1.5 Torr He and 298 K. The pink line indicates 52% of the total reaction exothermicity (124.9 kJ mol^{-1}) which is the proportion of the energy measured to go into the H_2O by Butkovskaya and Setser.[52]

The calculated dissociation yields were found to be dependent upon both pressure and the value used for the energy transfer parameter $<\Delta E_{down}>$. Further details are available in the ESI. It was found that the CH_3 yield decreases with both increasing pressure and $<\Delta E_{down}>$and this can readily rationalized in terms of the increased rate of collisional stabilization of the activated CH_3CO fragments which reduces the amount of prompt fragmentation.

Two previous studies on reaction 1 have looked for methyl radicals. Wang et al.[22] used tuneable diode laser IR absorption to monitor the production of ground vibrational state methyl radicals from reaction 1, calibrated by the known CH_3 yield from the $O(^1D)$ reaction with methane. A prompt methyl signal was observed attributed to reaction 5 with a slower growth of methyl radicals from reaction 1 on the 100's of μsec timescale. It is not clear from the paper how the significant loss of methyl radicals from radical-radical processes, occurring on a similar timescale to methyl production or the production of vibrationally excited methyl radicals has been taken into account and therefore it is possible that the reported methyl yield at ~14 Torr of helium (5%) may be an underestimate of the yield. Using the MESMER input optimized to produce ~13.5 % CH_3 yield at 1.5 Torr of helium, it was found that increasing the pressure to 14 Torr reduced the calculated methyl yield to approximately 12 %.

Cameron et al.[21] used UV absorption (200 – 240 nm) to observe acetyl and methyl radicals produced in reaction 1. The acetyl absorption spectrum is quite broad and featureless in this region, whereas in contrast, the ground state methyl absorption peaks sharply at ~216 nm. High concentrations of acetaldehyde were used and therefore there is no time resolution in the production of acetyl or methyl radicals. Methyl radicals were observed, but Cameron et al.[21] suggest that this can be attributed to acetaldehyde photolysis and the maximum yield of methyl radicals was set at 3% for the 60 Torr (N_2) experiments. Uncertainties in accounting for the CH_3 photolysis yield or possible contributions from vibrationally excited species could increase methyl yields and MESMER calculations suggest a reduced methyl yield of 11% for 60 Torr of N_2 compared to our PIMS experiments (~1.5 Torr He).

Neither of the previous studies on methyl radical production are ideal to determine methyl yields in the region of 5 – 15%, and indeed, were not designed to achieve such precision. At the time it had been proposed that addition-elimination reactions might be the dominant pathways for the reaction of OH with acetaldehyde and both studies, this work and that of D'Anna et al.[26] , clearly demonstrate that methyl radical production is a minor channel in reaction 1.

Despite being a minor channel, so that atmospheric implications are limited, the observation of methyl radicals from reaction 1 raises some interesting points about the mechanism of abstraction reactions and may have implications for low temperature combustion. Conventionally in an abstraction reaction, reaction exothermicity is preferentially channeled into the newly formed bond with the acetyl fragment being a 'spectator' of the reaction. The observation of ~ 15% fragmentation of the acetyl radical, with fragmentation requiring greater than 50% of the reaction exothermicity to be channeled into acetyl, demonstrates that the energy is distributed more statistically. A completely statistical distribution of energy would preferentially excite the acetyl fragment (12 modes vs 3 modes) and lead to almost complete acetyl fragmentation. Clearly both the classical 'dynamic' and 'statistical' models of partitioning energy do not agree with our experimental observations or those of other workers. Butkovskaya and Setser[52] have studied the IR chemiluminescence arising from reaction 1 and several other abstraction reactions. Based on their observations they calculate that 52% of the reaction exothermicity is channeled into vibrational excitation of the water. Figure 7 shows a line corresponding to 52% of the total exothermicity and it can be observed that the peak in the H_2O vibrational distribution from this work is consistent with the observations of Butkovskaya and Setser. Their observations also point to significant differences in the mechanism of OH abstraction reactions between alkanes and carbonyls. In the latter case a smaller fraction of the reaction exothermicity (typically ~50% vs 70%) is channeled into vibration/bending of the water molecule and the ratio of vibrational:bending is much

more statistical following abstraction from a carbonyl species. The potential for post-reaction complexes between the water and carbonyl radicals to facilitate widening the distribution of energy was postulated as one possible explanation. Our observations on the degree of OH recycling in the presence of oxygen following OH reaction with methylglyoxal and glyoxal are also only consistent with a significant fraction of the reaction exothermicity being present in the $CH_3C(O)CO$ and $HC(O)CO$ fragments respectively.[27,30]

The implications of this study could be significant in low temperature combustion, particularly under oxyfuel combustion conditions (combustion in pure oxygen to facilitate post combustion CO_2 capture[53]). Aldehydes are known to be important intermediates in the combustion of alcohols and Kaiser et al.[54] have modeled the chemistry of acetaldehyde oxidation under typical low temperature combustion conditions (T<1000 K). At temperatures below 750 K chain branching can occur via reactions 2a, 17 and 18:

$$CH_3CO + O_2 \rightarrow CH_3C(O)O_2 \quad (2a)$$

$$CH_3C(O)O_2 + CH_3CHO \rightarrow CH_3C(O)O_2H + CH_3CO \quad (17)$$

$$CH_3C(O)O_2H \rightarrow CH_3 + CO_2 + OH \quad (18)$$

Reaction 2a will be in competition with the chain propagation step 2b

$$CH_3CO + O_2 \rightarrow OH + \text{co-products} \quad (2b)$$

with the likely co-product being a lactone which decomposes to HCHO and CO. MESMER calculations emphasize the importance of 'well-skipping' reactions in such $R + O_2$ systems[55] and well-skipping will be enhanced with vibrational excitation of the R radical. Our results indicate significant vibrational excitation of the acetyl fragment following reaction 1 and, particularly under oxyfuel combustion where there will be less vibrational relaxation, the fraction of chain branching, reactions 2a, 17, 18, versus chain propagation, reaction 2b, will change.

To explore how the importance of the well-skipping reactions changes with the amount of internal energy in the CH_3CO fragment, calculations have been performed upon the $CH_3CO + O_2$ reaction with the CH_3CO radical initiated with varying amounts of excess energy using a prior distribution. From these calculations it is found that as the internal energy of the CH_3CO radical is increased, well-skipping reactions from the excited CH_3CO increase the yield of the lactone + OH product channel relative to stabilization of the RO_2 species $CH_3C(O)OO$. Figure 8 shows the calculated yield of OH versus the internal energy in the CH_3CO, where here the internal energy of the CH_3CO is associated with the peak of the distribution of energies. Such enhancements of well-skipping to yield the

chain propagation products compared to stabilization to give acetyl peroxy radicals and potential chain branching via reactions 17 and 18, could influence modeled ignition delays for ethanal combustion.

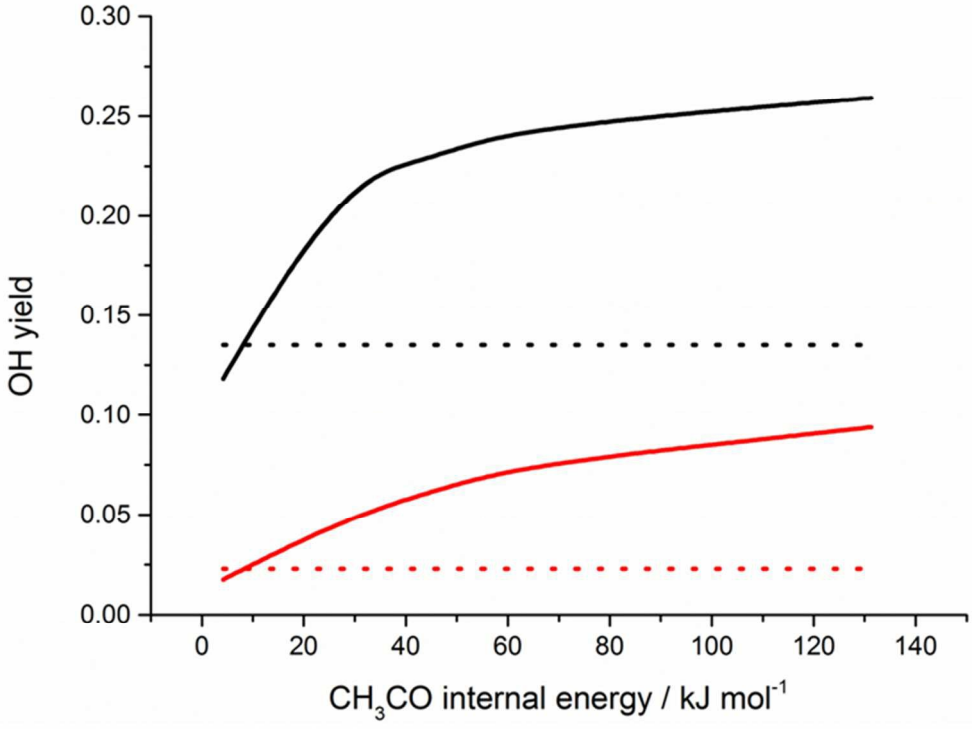

Figure 8. Calculated OH yields from the $CH_3CO + O_2$ reaction at 100 (black) and 760 (red) Torr air and 298 K. In these calculations the CH_3CO was initialized with a prior distribution as described above, and the excess energy available was varied. The internal energy on the x axis is given by the peak in the CH_3CO initial distribution of energies. The dotted lines correspond to OH yields under Boltzmann conditions at 298 K.

ASSOCIATED CONTENT

Supporting Information. Additional details on experimental techniques, the calibration methods, the investigation of possible interferences from secondary chemistry and the pressure dependence of calculated CH_3 yields. This material is available free of charge via the Internet at http://pubs.acs.org.

AUTHOR INFORMATION

Corresponding Authors

* Paul Seakins, School of Chemistry, University of Leeds, Leeds, LS2 9JT, UK, p.w.seakins@leeds.ac.uk. Mark Blitz, School of Chemistry, University of Leeds, Leeds, LS2 9JT, UK, m.blitz@leeds.ac.uk.

Present Addresses

† Current address, Argonne National Laboratory, Argonne, IL, USA.[+] Escuela de Ingenieria Industrial de Toledo, Toledo, Spain. ‡ University of Bristol, Canntock's Close, Bristol, UK. # Institute of Chemistry, Eotvos University, Budapest, Hungary.

Author Contributions

The manuscript was written through contributions of all authors.

ACKNOWLEDGMENT

The authors are grateful to NERC for studentships for NUMH, and JPAL, to EPSRC for a studentship for SAC (Grant GR/T28560/01) and support for RJS (Grant EP/J010871/1).

TOC

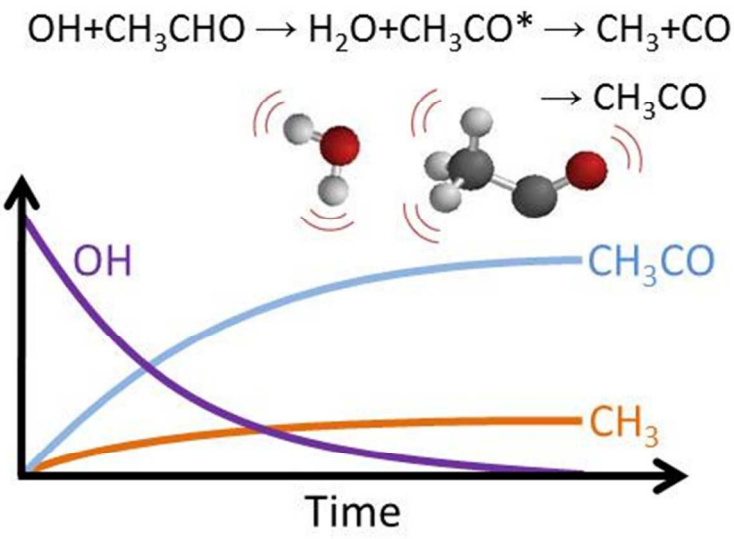

REFERENCES

1. D. J. Luecken, W. T. Hutzell, M. L. Strum and G. A. Pouliot, *Atmos. Environ.*, 2012, **47**, 477-490.
2. S. A. Carr, M. A. Blitz and P. W. Seakins, *J. Phys. Chem. A*, 2011, **115**, 3335-3345.
3. G. Karavalakis, T. D. Durbin, M. Shrivastava, Z. Q. Zheng, M. Villela and H. J. Jung, *Fuel*, 2012, **93**, 549-558.
4. D. B. Millet, E. Apel, D. K. Henze, J. Hill, J. D. Marshall, H. B. Singh and C. W. Tessum, *Environmental Science & Technology*, 2012, **46**, 8484-8492.
5. P. Dagaut and C. Togbe, *Fuel*, 2008, **87**, 3313-3321.
6. B. Q. He, M. B. Liu, J. Yuan and H. Zhao, *Fuel*, 2013, **108**, 668-674.
7. K. A. Read, L. J. Carpenter, S. R. Arnold, R. Beale, P. D. Nightingale, J. R. Hopkins, A. C. Lewis, J. D. Lee, L. Mendes and S. J. Pickering, *Environmental Science & Technology*, 2012, **46**, 11028-11039.
8. Y. J. Zhang, Y. J. Mu, P. Liang, Z. Xu, J. F. Liu, H. X. Zhang, X. K. Wang, J. Gao, S. L. Wang, F. H. Chai and A. Mellouki, *Atmos. Environ.*, 2012, **59**, 186-191.
9. H. K. Wang, C. H. Huang, K. S. Chen and Y. P. Peng, *Aerosol Air Qual. Res.*, 2010, **10**, 559-570.
10. S. M. Correa, G. Arbilla, E. M. Martins, S. L. Quiterio, C. D. Guimaraes and L. V. Gatti, *Atmos. Environ.*, 2010, **44**, 2302-2308.
11. E. C. Fortner, J. Zheng, R. Zhang, W. B. Knighton, R. M. Volkamer, P. Sheehy, L. Molina and M. Andre, *Atmos. Chem. Phys.*, 2009, **9**, 467-481.
12. E. P. A. US, *Health Assessment Document for Acetaldehyde.*, Environmental Criteria and Assessment Office, Office of Health and Environmental Assessment, Office of Research and Development, Research Triangle Park, NC, 1987.
13. R. Atkinson, D. L. Baulch, R. A. Cox, J. N. Crowley, R. F. Hampson, R. G. Hynes, M. E. Jenkin, M. J. Rossi and J. Troe, *Atmos. Chem. Phys.*, 2004, **4**, 1461-1738.
14. S. P. Sander, R. R. Friedl, J. P. D. Abbatt, J. Barker, D. M. Golden, C. E. Kolb, M. J. Kurylo, G. K. Moortgat, P. H. Wine, R. E. Huie and V. L. Orkin, *Chemical kinetics and photochemical data for use in atmospheric studies - Evaluation 17*, Jet Propulsion Laboratory, Pasadena CA, 2011.
15. M. Wollenhaupt, S. A. Carl, A. Horowitz and J. N. Crowley, *J. Phys. Chem. A*, 2000, **104**, 2695-2705.
16. G. Vasvari, I. Szilagyi, A. Bencsura, S. Dobe, T. Berces, E. Henon, S. Canneaux and F. Bohr, *Phys. Chem. Chem. Phys.*, 2001, **3**, 551-555.
17. P. H. Taylor, M. S. Rahman, M. Arif, B. Dellinger and P. Marshall, *Proceedings of the Combustion Institute*, 1996, **26**, 497-504.
18. S. Vandenberk and J. Peeters, *Journal of Photochemistry and Photobiology a-Chemistry*, 2003, **157**, 269-274.
19. S. Vandenberk, L. Vereecken and J. Peeters, *Phys. Chem. Chem. Phys.*, 2002, **4**, 461-466.
20. N. I. Butkovskaya, A. Kukui and G. Le Bras, *J. Phys. Chem. A*, 2004, **108**, 1160-1168.
21. M. Cameron, V. Sivakumaran, T. J. Dillon and J. N. Crowley, *Phys. Chem. Chem. Phys.*, 2002, **4**, 3628-3638.
22. J. Wang, H. L. Chen, G. P. Glass and R. F. Curl, *J. Phys. Chem. A*, 2003, **107**, 10834-10844.
23. R. J. Shannon, M. A. Blitz, A. Goddard and D. E. Heard, *Nat. Chem.*, 2013, **5**, 745-749.

24. R. J. Shannon, R. L. Caravan, M. A. Blitz and D. E. Heard, *Phys. Chem. Chem. Phys.*, 2014, **16**, 3466-3478.
25. E. Vohringer-Martinez, B. Hansmann, H. Hernandez, J. S. Francisco, J. Troe and B. Abel, *Science*, 2007, **315**, 497-501.
26. B. D'Anna, V. Bakken, J. A. Beukes, C. J. Nielsen, K. Brudnik and J. T. Jodkowski, *Phys. Chem. Chem. Phys.*, 2003, **5**, 1790-1805.
27. M. T. Baeza-Romero, D. R. Glowacki, M. A. Blitz, D. E. Heard, M. J. Pilling, A. R. Rickard and P. W. Seakins, *Phys. Chem. Chem. Phys.*, 2007, **9**, 4114-4128.
28. J. C. Polanyi, *Science*, 1987, **236**, 680-690.
29. J. Mendes, C. W. Zhou and H. J. Curran, *J. Phys. Chem. A*, 2014, **118**, 12089-12104.
30. J. Lockhart, M. Blitz, D. Heard, P. Seakins and R. Shannon, *J. Phys. Chem. A*, 2013, **117**, 11027-11037.
31. J. V. Michael, D. G. Keil and R. B. Klemm, *J. Chem. Phys.*, 1985, **83**, 1630-1636.
32. S. A. Carr, D. R. Glowacki, C. H. Liang, M. T. Baeza-Romero, M. A. Blitz, M. J. Pilling and P. W. Seakins, *J. Phys. Chem. A*, 2011, **115**, 1069-1085.
33. G. da Silva, *Phys. Chem. Chem. Phys.*, 2010, **12**, 6698-6705.
34. M. T. Baeza-Romero, M. A. Blitz, A. Goddard and P. W. Seakins, *Int. J. Chem. Kinet.*, 2012, **44**, 532-545.
35. M. A. Blitz, A. Goddard, T. Ingham and M. J. Pilling, *Rev. Sci. Instrum.*, 2007, **78**.
36. D. R. Glowacki, C. H. Liang, C. Morley, M. J. Pilling and S. H. Robertson, *J. Phys. Chem. A*, 2012, **116**, 9545-9560.
37. P. A. Cleary, M. T. B. Romero, M. A. Blitz, D. E. Heard, M. J. Pilling, P. W. Seakins and L. Wang, *Phys. Chem. Chem. Phys.*, 2006, **8**, 5633-5642.
38. D. R. Glowacki, J. Lockhart, M. A. Blitz, S. J. Klippenstein, M. J. Pilling, S. H. Robertson and P. W. Seakins, *Science (Washington, D. C., 1883-)*, 2012, **337**, 1066-1067.
39. M. Baasandorj, D. K. Papanastasiou, R. K. Talukdar, A. S. Hasson and J. B. Burkholder, *Phys. Chem. Chem. Phys.*, 2010, **12**, 12101-12111.
40. P. D. Lightfoot, S. P. Kirwan and M. J. Pilling, *J. Phys. Chem.*, 1988, **92**, 4938-4946.
41. S. A. Carr, M. T. Baeza-Romero, M. A. Blitz, M. J. Pilling, D. E. Heard and P. W. Seakins, *Chem. Phys. Lett.*, 2007, **445**, 108-112.
42. G. Kovacs, J. Zador, E. Farkas, R. Nadasdi, I. Szilagyi, S. Dobe, T. Berces, F. Marta and G. Lendvay, *Physical Chemistry Chemical Physicis*, 2007, **9**, 4142-4154.
43. G. S. Tyndall, J. J. Orlando, T. J. Wallington and M. D. Hurley, *Int. J. Chem. Kinet.*, 1997, **29**, 655-663.
44. M. Baer and W. L. Hase, *Unimolecular Reaction Dynamics*, Oxford University Press, Oxford, 1986.
45. Y. Zhao and D. G. Truhlar, *Theor. Chem. Acc.*, 2008, **120**, 215-241.
46. M. J. Frisch, G. W. Trucks, H. B. Schlegel, G. E. Scuseria, M. A. Robb, J. R. Cheeseman, G. Scalmani, V. Barone, B. Mennucci, G. A. Petersson, H. Nakatsuji, M. Caricato, X. Li, H. P. Hratchian, A. F. Izmaylov, J. Bloino, G. Zheng, J. L. Sonnenberg, M. Hada, M. Ehara, K. Toyota, R. Fukuda, J. Hasegawa, M. Ishida, T. Nakajima, Y. Honda, O. Kitao, H. Nakai, T. Vreven, J. Montgomery, J. A.;, J. E. Peralta, F. Ogliaro, M. Bearpark, J. J. Heyd, E. Brothers, K. N. Kudin, V. N. Staroverov, R. Kobayashi, J. Normand, K. Raghavachari, A. Rendell, J. C. Burant, S. S. Iyengar, J. Tomasi, M. Cossi, N. Rega, J. M. Millam, M. Klene, J. E. Knox, J. B. Cross, V. Bakken, C. Adamo, J. Jaramillo, R. Gomperts, R. E. Stratmann, O. Yazyev, A. J. Austin, R. Cammi, C. Pomelli, J. W. Ochterski, R. L. Martin, K. Morokuma, V. G. Zakrzewski,

G. A. Voth, P. Salvador, J. J. Dannenberg, S. Dapprich, A. D. Daniels, Ö. Farkas, J. B. Foresman, J. V. Ortiz, J. Cioslowski and D. J. Fox, *Gaussian 09, Revision **A.1***, Gaussian, Inc., Wallingford CT2009.

47. H. J. Werner, P. J. Knowles, G. Knizia, F. R. Manby and M. Schutz, *Wiley Interdiscip. Rev.-Comput. Mol. Sci.*, 2012, **2**, 242-253.
48. A. W. Jasper and J. A. Miller, *J. Phys. Chem. A*, 2011, **115**, 6438-6455.
49. N. J. B. Green and S. H. Robertson, *Chem. Phys. Lett.*, 2014, **605**, 44-46.
50. K. Lorenz, D. Rhasa, R. Zellner and B. Fritz, *Ber. Bunsen-Ges. Phys. Chem. Chem. Phys.*, 1985, **89**, 341-342.
51. E. Delbos, C. Fittschen, H. Hippler, N. Krasteva, M. Olzmann and B. Viskolcz, *J. Phys. Chem. A*, 2006, **110**, 3238-3245.
52. N. I. Butkovskaya and D. W. Setser, *J. Phys. Chem. A*, 2000, **104**, 9428-9435.
53. M. E. Boot-Handford, J. C. Abanades, E. J. Anthony, M. J. Blunt, S. Brandani, N. Mac Dowell, J. R. Fernandez, M. C. Ferrari, R. Gross, J. P. Hallett, R. S. Haszeldine, P. Heptonstall, A. Lyngfelt, Z. Makuch, E. Mangano, R. T. J. Porter, M. Pourkashanian, G. T. Rochelle, N. Shah, J. G. Yao and P. S. Fennell, *Energy & Environmental Science*, 2014, **7**, 130-189.
54. E. W. Kaiser, C. K. Westbrook and W. J. Pitz, *Int. J. Chem. Kinet.*, 1986, **18**, 655-688.
55. A. J. Eskola, S. A. Carr, R. J. Shannon, B. Wang, M. A. Blitz, M. J. Pilling, P. W. Seakins and S. H. Robertson, *J. Phys. Chem. A*, 2014, **118**, 6773-6788.